Scheme IV. Pair Mechanism for Allylperoxyl Rearrangement

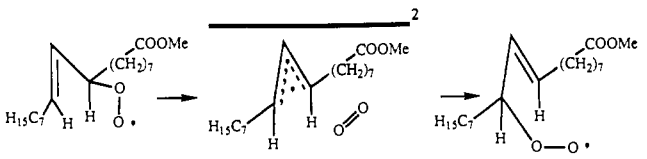

rearrangement at 40 °C compared to that observed at room temperature[7], an observation which is consistent with pair escape competing successfully with pair collapse.

The pair mechanism suggested by theory and the stereochemistry observed in the experiments stimulated us to investigate the structure of allyl radicals in some detail. A pyramidal allyl or one that had an energy barrier separating a pyramidal allyl and a planar structure might give rise to a facial bias in the addition of oxygen to the radical, especially if inversion of the radical were slow relative to encounter and reaction with atmospheric oxygen. The structures of several different allyl structures were calculated (Table III). Sterically hindered radicals such as **Q** and **R** exhibit slight twisting of the plane containing the radical center, i.e., the $C_2C_3C_4C_5$ dihedral angle is about 2°. But each radical investigated was planar at the radical center(s): the sum of the bond angles around the carbons with high spin density was 360°. No pyramidalization of the radical center was therefore observed. In general, both C_2 and C_4 exhibit spin densities of essentially equal magnitudes, with a very slightly greater density on the more substituted carbon (e.g., in structure **O**, C_2 has spin density of 1.023, while C_4 has 1.014.)

Thus our conclusion remains that the selectivity of the rearrangement of the allylperoxyl radical results from a cage effect wherein the diffusion of the allyl radical-oxygen pair is prevented due to caging by the solvent.

Acknowledgment. We acknowledge financial assistance provided by a NATO Grant for International Collaborative Research (to L.R.C.B. and N.A.P.). The financial support of the Natural Sciences and Engineering Research Council of Canada (to R.J.B.) and the Research Fund of MSVU (to S.L.B.) is also gratefully acknowledged.

Magic Angle (54.7°) Gradient and Minimal Surfaces in Quadruple Micellar Helices

Jürgen Köning,[†] Christoph Boettcher,[†,‡] Hanspeter Winkler,[‡] Elmar Zeitler,[‡] Yeshayahu Talmon,[§] and Jürgen-Hinrich Fuhrhop*[,†]

Contribution from the Institut für Organische Chemie der Freien Universität Berlin, Takustrasse 3, 1000 Berlin 33, Germany, Fritz-Haber-Institut der Max-Planck-Gesellschaft, Faradayweg 4-6, 1000 Berlin 33, Germany, and Department of Chemical Engineering, Technion-Israel Institute of Technology, Haifa, 32000, Israel. *Received June 2, 1992*

Abstract: The first self-organized quadruple helices consisting of nonpolymeric material have been obtained from *N*-octyl- and *N*-dodecyl-D-gluconamides in water. They have been characterized by electron microscopy, image analysis, and computer modelling. The pitch of the helices is equal to (2π × molecular bilayer diameter); their gradient conforms with the magic angle (54.7°). The quadruple helices rearrange in aqueous gels to a single helix made of circular 4-fold layers of molecules, a pitch of 7.4 nm, and a gradient of 82 ± 3°. This quadruple layer may already contain head-to-tail oriented molecules, which are exclusively found in the final crystal sheets. The process of crystallization, from highly curved micellar fibers to planar crystal sheets, proceeds on minimal sufaces.

Molecular assemblies of amphiphiles in water are organized by the same physical forces that enforce order in proteins, namely, the hydrophobic effect, hydrogen bonding, steric repulsion, and charge interactions. Similar molecular shapes are therefore observed in molecular assemblies[1] and proteins,[2] in particular globules, sheets, and helical fibers. The tightness of the arrangements in assemblies and proteins, however, is different. The relative arrangement of the monomers in proteins is largely determined by the covalent backbone; e.g., the smallest possible loop is usually preferred in helices. The loose attachment of the monomers in assemblies, on the other hand, reflects more directly the impact of repulsive and attractive physical forces. From detailed analysis of complex structures of such assemblies, one may therefore learn more about the action of physical forces between molecules. We report here for the first time on micellar quadruple helices, which incline at the magic angle, thereby minimizing the dielectric energy associated with order electric polarization of oriented quadrupolar systems. Furthermore, we have evaluated a rearrangement of these quadruple helices to a single right-handed helical tube made of a molecular 4-fold layer, which has the appearance of elongated staples of toroids in electron micrographs.

Results

Electron Microscopy. Micellar fibers made of *N*-alkylglyconamides have been characterized by us earlier with the aid of electron microscopy.[3,4] *N*-Octyl- and *N*-dodecylgluconamides[3] (**1a,b**) as well as *N*-octadecylmannonamides[5] were supposed to produce double helices with bulges and knots ("bulgy helices") at room temperature in the presence of 1% phosphotungstate. Addition of other electrolytes usually leads to the formation of microcrystalline platelets. A new series of negative stain electron

* To whom correspondence should be addressed.
† Institut für Organische Chemie.
‡ Fritz-Haber-Institut.
§ Technion.

(1) (a) Fuhrhop, J.-H.; Svenson, S.; Boettcher, C.; Bach, R.; Schnieder, P. In *Molecular Mechanism in Bioorganic Processes*; Bleasdale, C., Golding, B., Eds.; Royal Society of Chemistry: Cambridge, 1990; p 65. (b) Fuhrhop, J.-H.; Krull, M. In *Modern Trends in Supramolecular Chemistry*; Schneider, H.-J.; Dürr, H., Eds.; VCH: Weinheim, 1991; p 223.
(2) (a) Richardson, J. S. *Adv. Protein Chem.* **1981**, *34*, 167. (b) Rassmann, M. G.; Argos, P. *Annu. Rev. Biochem.* **1981**, *50*, 497. (c) Dickerson, R. E.; Geis, I. *Hemoglobin*; Benjamin: Menlo Park, CA, 1983; p 125 ff.
(3) Fuhrhop, J.-H.; Schnieder, P.; Rosenberg, J.; Boekema, E. *J. Am. Chem. Soc.* **1987**, *109*, 3387.
(4) Fuhrhop, J.-H.; Schnieder, P.; Boekema, E.; Helfrich, W. *J. Am. Chem. Soc.* **1988**, *110*, 2861.
(5) Fuhrhop, J.-H.; Svenson, S.; Boettcher, C.; Rössler, E.; Vieth, H.-M. *J. Am. Chem. Soc.* **1990**, *112*, 4307.

0002-7863/93/1515-693$04.00/0

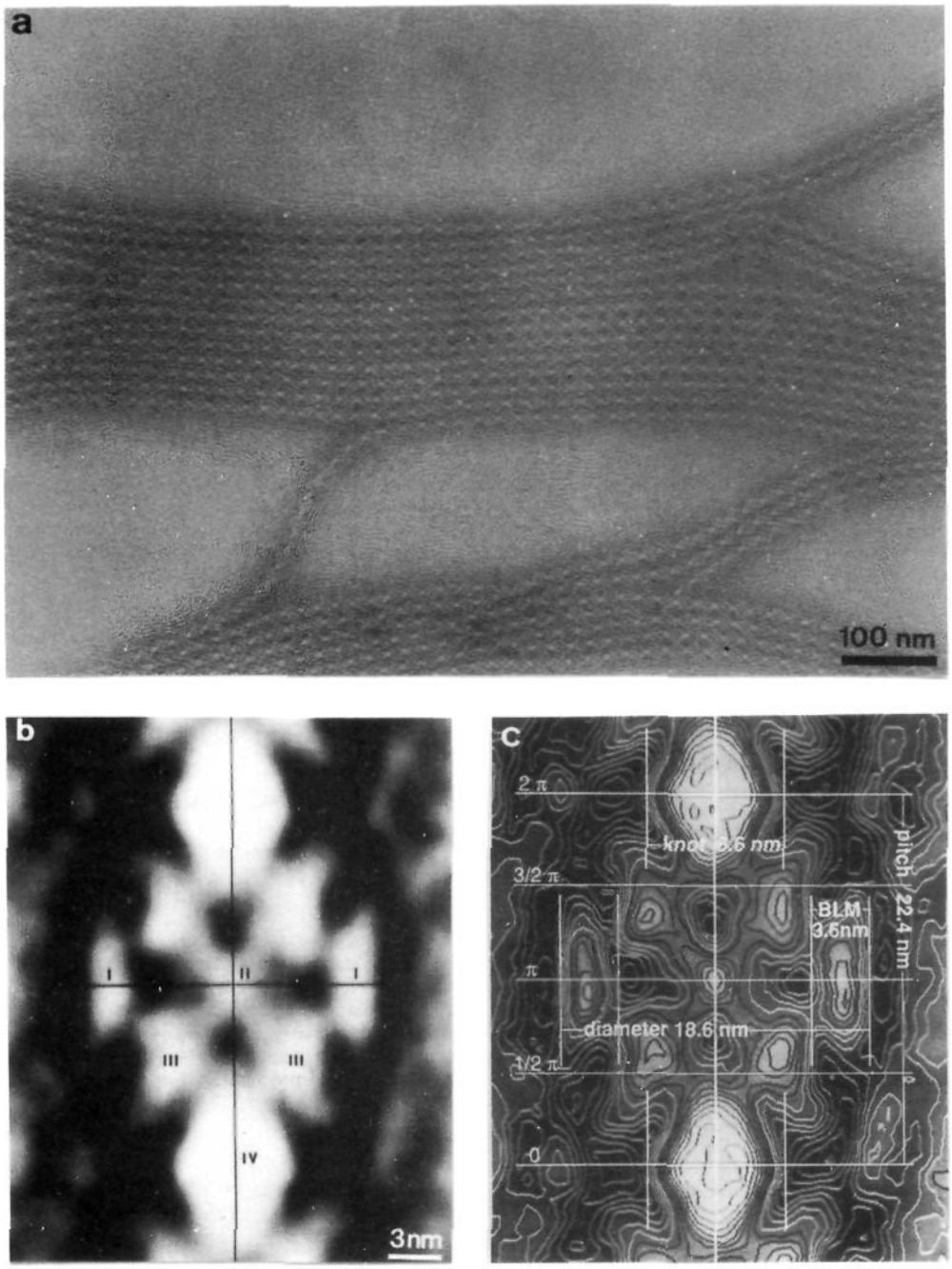

Figure 1. (a) Electron micrograph of a two-dimensional array of *N*-octyl-D-gluconamide (**1a**) fibers, negatively stained with 2% phosphotungstate. (b) Image-processed repetitive unit of the above molecular assembly. The numbers indicate maxima of mass distributions (see Modelling). (c) Contour line diagram of Figure 1b.

micrographs of almost crystalline 2D arrays of fibers (Figure 1a) was taken. This allowed image processing of the structure pattern. It revealed additional electron density in the center of the bulges. Applying cross-correlation averaging with the image-processing software (SEMPER)[6] to 165 motifs of constant period length (see Experimental Section) yielded the fiber pattern of Figure 1b, which is also presented as a profile line overlay in Figure 1c. The pattern reveals most details within the bulges. The following quantitative data were extracted: (i) the pitch along the *z*-axis is 22.4 ± 0.50 nm, (ii) the maximum diameter of the bulge diameter is 18.6 ± 0.4 nm, (iii) the knot diameter is 8.6 ± 0.2 nm, and (iv) the diameter of the elliptical maxima I (Figure 1c) is 3.6 ± 0.2 nm. This corresponds approximately to the length of two molecules of *N*-octylgluconamide in its crystal structure.[7] Furthermore, there are two distinct C_2-symmetry axes in the direction of the *z*-axis and perpendicular to it.

We then attempted to obtain a 3D reconstruction of the fiber by an electron microscopical tilt series in steps of 8° at angles between −48° and +56°. A narrowing of the apparent fiber diameter was strikingly obvious at 48° as compared to 0° (Figure 2a). The 3D structure shown in Figure 2b which resulted from the computer-aided image analysis and reconstruction of the tilt series shows a considerable flattening of the micellar fibers, which is a result of both lipid fiber deformation and missing tilt angles above 56°. Similar flattenings of other water-containing materials

(6) (a) Misell, D. L. *Image Analysis*; North Holland: Amsterdam, 1978. (b) Saxton, W. O.; Koch, T. L. *J. Micros.* (*Oxford*) **1982**, *127*, 69.

(7) Zabel, V.; Müller-Fahrnow, A.; Hilgenfeld, R.; Saenger, W.; Pfannenmüller, B.; Enkelmann, V.; Welte, W. *Chem. Phys. Lipids* **1985**, *39*, 313.

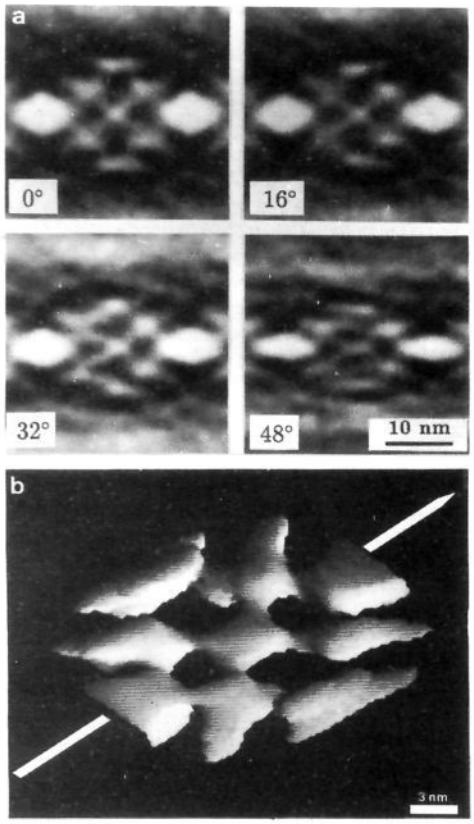

Figure 2. (a) Image-processed repetitive units at selected tilt angles (compare Figure 1b). (b) 3D reconstruction of a repetitive unit as obtained from the tilt series.

have been reported in the literature.[8]

We therefore studied the fibers after a cryomicroscopic preparation in a controlled environment vitrification system (CEVS).[9] This technique also allows the omission of a staining with heavy metal salts. The fibers reproduced in Figure 3a were prepared at 70 °C, a temperature slightly below their melting point. They were then solidified within a few milliseconds in liquid ethane. The fibers were thus entrapped in vitreous ice, presumably without any change of their native 3D structure. The bulgy helices were indeed detectable in the electron micrographs, but the low contrast of the pure organic material required strong defocussing. The modulation of high spatial frequncies and an increased radiation damage both lowered the resolution. In the presence of 1% sodium dodecylsulfate (SDS),[5] a 2D-crystalline arrangement of the fibers was again obtained (Figure 3b) and allowed image analysis (Figure 3c). Similar bulgy helices as in the stained material were found. The low resolution, however, did not allow the detection of extra electron density in the center of the bulges.

Helices made of the homologue *N*-dodecylgluconamide (**1b**) were investigated again in negatively stained preparations (Figure 4a). The mass distribution clearly differs from that of the *N*-octyl compound. The fibers in the bulge region are much thicker than a molecular bilayer, and no extra material appears in the center of the bulges. A data set is again obtained from the contour line overlay (Figure 4a): (i) a pitch of 27.1 ± 0.5 nm, (ii) a bulge width of 22.1 ± 0.5 nm, and (iii) a knot diameter of 11.6 ± 0.3 nm. The bilayer thickness cannot be found in this structural display. It should be 1.0 nm (=eight methylene groups = 8 × 0.125 nm) thicker than the octyl homologue and would correspond to 4.6 ± 0.2 nm. It is not possible to rationalize the enormous differences to the corresponding pattern of the octylamide (Figure 1c) just by inspection of the electron micrographs. In the next section, it will be shown by analytical modelling procedures that differences in fiber orientations are responsible for these structural deviations.

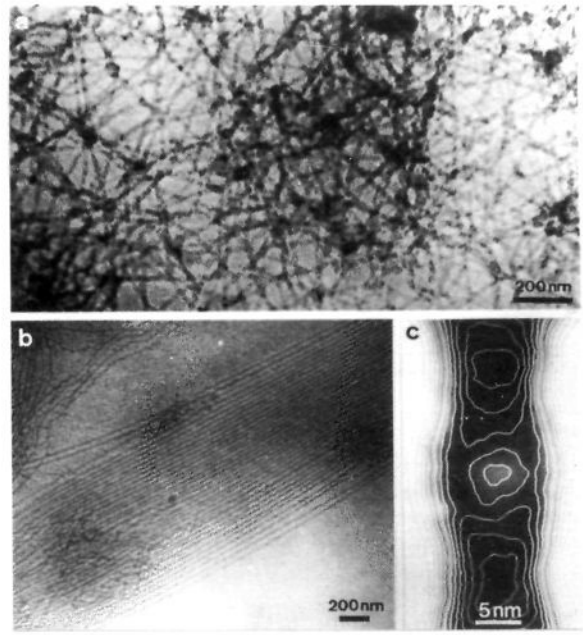

Figure 3. (a) *N*-Octylgluconamide fibers as obtained at 70 °C (CEVS) followed by vitrification (without stain). (b) Same as above in presence of 0.4% SDS. (c) Image-processed contour-line diagram showing the repetitive unit of the fibers.

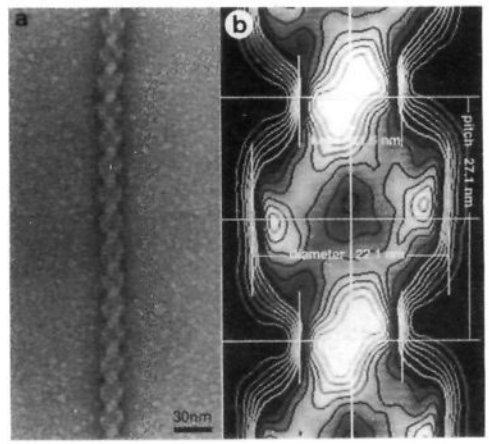

Figure 4. (a) Electron micrograph of a single fibrous molecular assembly of *N*-dodecyl-D-gluconamide (**1b**), negatively stained with 2% phosphotungstate. (b) Contour-line diagram of an image-processed unit of this fiber.

Upon cooling, another type of molecular assembly is formed within a few minutes, if phosphotungstate is omitted during the process of fiber formation. Thicker, rodlike fibers could be obtained in pure form. They quickly rearrange to form crystalline platelets, in which all molecules are in head-to-tail arranged sheets.[7] The spontaneous re-formation of thinner fibers was never observed. The same[10] or similar[11] fibers have been already demonstrated by other authors. Vitrified and freeze etched, they showed a diameter of 27.4 ± 2 nm and striations with a regular repeat distance of 7.4 ± 4 nm. The latter are aligned at an angle of 82 ± 3° in respect to the fiber axis (Figure 5). Occasional cross-sectional views revealed a cavity in the center of the rods with a diameter of approximately 12 nm. The thickness of the wall amounts to 7.0 ± 2 nm.

(8) Kistler, J.; Kellenberger, E. *J. Ultrastruct. Res.* **1977**, Res. *59*, 70.
(9) Bellare, J. R.; Davis, H. T.; Scriven, L. E.; Talmon, Y. *J. Electron Microsc. Tech.* **1988**, *10*, 87.
(10) Pfannemüller, B.; Welte, W. *Chem. Phys. Lipids* **1985**, *37*, 227.
(11) Nakashima, N.; Asakuma, S.; Kunitake, T. *J. Am. Chem. Soc.* **1985**, *107*, 509.

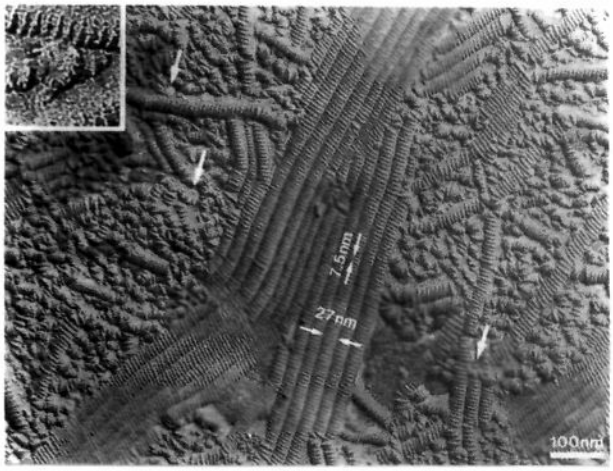

Figure 5. Electron micrograph of a freeze-etched preparation of the tubular assemblies of gluconamide **1a**. Arrows point to cross-sectional views. The enlarged inset (12×) shows such a cross section.

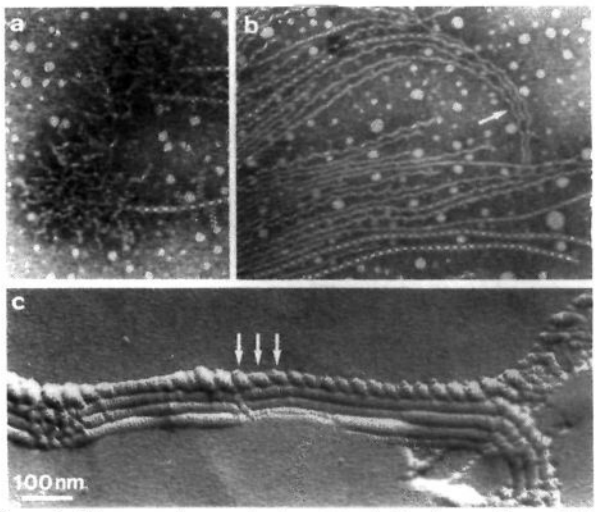

Figure 6. Electron micrographs show (a) micellar clusters from which bulgy helices grow, (b) coiled helices connected to straight bulgy helices, and (c) coiled tubules. (a, b) are negatively stained with phosphotungstate; (c) is shadowed with Pt/C.

Finally we wish to mention occasional observations of micellar fiber structures. They include micellar clusters from which bulgy helices grow (Figure 6a), coiled bulgy helices (Figure 6b), and coiled tubular rods (Figure 6c). The common trend in the development of aggregates is seen in a tendency to diminish curvature and to increase torsion with time.

Geometrical Analysis and Modelling. It was found to be impossible to identify the 3D structure of the fiber directly using the electron microscopic images reproduced in Figures 1 and 2. We therefore used a computer-aided geometrical reconstruction for analysis and modelling of these complex fibers.

From the uniform appearance of the supramolecular structure, we first concluded that the repetitive unit must be composed of regular subunits. We then continued along the following pathway: (i) the molecular bilayer and its geometric shape were determined; (ii) the number N of strands was established; (iii) the arrangement of individual strands within the fiber bundle was analyzed, including positions of the strand axes, phase shifts, and packing symmetries. Finally, (iv) experimental data of the contour line overlay (Figure 1c) were used to model 3D structures of the fiber.

The thinnest part of the fiber is found at the maxima I (Figure 1b). Their diameter of 3.6 nm provides evidence for the molecular bilayer as the smallest unit. The molecular length of the all-trans conformation of N-octylgluconamide can be obtained from the crystal structure as 1.9 nm. Steric repulsion of the syn-axial hydroxyl groups at C2 and C4 leads to a kink and causes a shortening to 1.7 nm. The electron microscopic measure or 3.6 nm thus corresponds to a molecular bilayer which should be of circular cross section.

From the occurrence of two C_2-symmetry axes parallel and orthogonal to the z-axis, we derive the following: (i) the 3D arrangement of the single strands is of even-numbered symmetry with respect to the fiber axis; (ii) the fiber is built by only one type of micellar helix; (iii) the number of helices should be the same in each xy cross section along the axis.

To deduce the number of strands, we first turned to the cross section at the maximum bulge diameter (positions I and II in Figure 1b). If one assigns the two outer elliptical areas (I) of BLM thickness to the turning points of a first pair of helices, the cross-shaped area (II) in the center of the pattern can be assigned to a second pair of helices crossing each other in the 2D image. Four individual helical strands are thus suggested. The same number is indicated by the four spots (III) with their cross-like extensions. They are therefore interpreted as superpositions of the first pair of helices moving from the outer elliptical spots (I) toward the knot region (IV) with the turning points of the second pair of helices. The thickness (8.6 nm) and the high density of lipid material of the main knot (IV) can then be assigned to a tightly packed arrangement of four, mutually interwoven strands. The presence of six or more individual strands can be excluded primarily because the space requirements of six strands with BLM thickness would be larger. Simulations of the density pattern of different 3D model structures (see below) allow for a more quantitative and direct comparison.

The regular sequence of knots and bulges necessitates the definition of four individual helix axes apart from and parallel to the central axis. The highly symmetrical arrangement of the quadruple helix can now be established in terms of regular phase differences $\Delta\varphi$ of $\pi/2$ between the individual helical strands. Expansion of the 2D image to 3D space yields either a C_4-symmetry (Figure 7a) or a C_2-symmetry (Figure 7b) around the z-axis:

axes	1	2	3	4
C_4; φ	0	$\pi/2$	π	$^3/_2\pi$
C_2; φ	0	$^3/_2\pi$	π	$^1/_2\pi$

We now determined the radii of the quadruple helix. The individual helix axes must all be equidistant to the central z-axis to reproduce the C_2- or C_4-symmetries. This distance determines the width of the quadruple helix and is called the "bulge radius". It is equivalent to the radius of a circle through all four helix axes. The bulge radius can be evaluated from the measures in Figure 1c as the difference between the horizontal radius of the knot and the bilayer radius (4.3−1.8 = 2.5 nm). The helix radius is then found to be 5.0 nm, corresponding to the radius of the quadruple helix at the bulges (=9.3 nm) minus the bulge (2.5 nm) and BLM (1.8 nm) radii. The numerical results of the electron microscopic data and the modelling procedure can now be summarized and scaled with the pitch equal to 4π:

mol length	BLM thickness	bulge radius	helix radius	pitch
1.8 nm	3.6 nm	2.5 nm	5.0 nm	22.4 nm
1 (1.01)	2 (2.02)	$\sqrt{2}$ (1.40)	$\sqrt{2}$ (2.81)	4π

With the proposed structure parametrization, the radii of the quadruple helix as well as its pitch relate in a simple geometric manner to the thickness of the molecular bilayer. An integral part of the parametrization is a pitch angle Θ of 54.74°. It is calculated by: $\Theta = \tan[2\pi \cdot \text{helix radius/pitch}] = \tan[\sqrt{2}]$ or 54.74°. This angle is depicted in the model structures reproduced in Figure 7.

The fibers interpenetrate in the knot regions (C4) or at $\pi/2$ and $3/2\pi$ (C2) of the pitch to a maximum of about 0.7 nm normal to the surface (see Figure 11). The maximum overlap therefore should involve strong interactions of the head groups. Rearrangements of the quadruple bilayer helices to quadruple layered single helices (see text below) probably start in these regions of interpenetration.

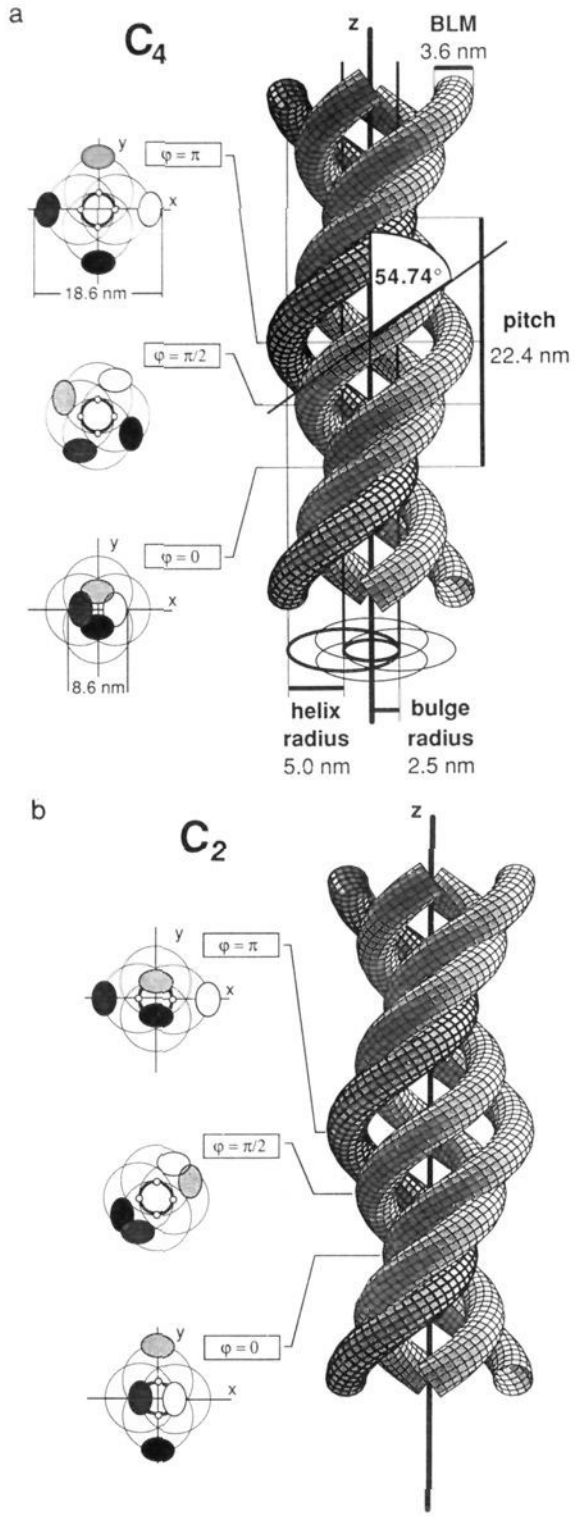

Figure 7. Computer graph of model structures of the quadruple helix made of *N*-octyl-D-gluconamide (**1a**) and cross sections at various pitch heights. The surface elements correspond approximately to single molecules: (a) C_4- and (b) C_2-symmetric structures. See text.

From *xy* cross sections of the parametrized 3D-model structures (Figure 7), a density profile has been calculated and superimposed on the image-analyzed electron micrograph (Figure 8). Shapes, positions, and intensities of the main maxima are as well reproduced as the areas of low lipid density. Mean positional deviations are between 0.2 and 0.7 nm and can be ascribed to the flattening of the fiber on the electron microscope's grid. Other radial parameters and packing symmetries have been evaluated and were

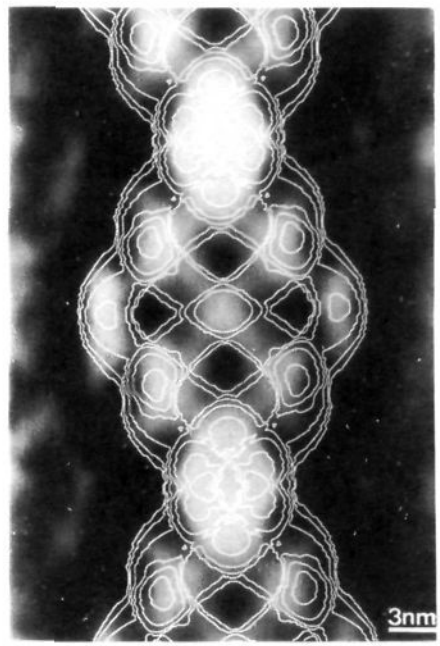

Figure 8. Calculated contour-line diagram of the models given in Figure 7 and as superimposed on the image-processed electron micrograph of this repetitive unit.

compared to experimental data. If, for example, the gradient angle is changed from 54.7° to 52°, the bulge diameter becomes too narrow by 13% or 1.9 nm, which is far beyond the limits of the *experimental fiber pattern*.

The resolution pathway for the *N*-dodecylgluconamide was very similar to the one described for the octyl homologue. This fiber was found to consist of the same quadruple helical fiber showing an incline of 54°. A different pattern occurred, because the data were obtained from a single elongated fiber which is turned by 45° with respect to the *z*-axis. This explains the observed absence of lipids in the center of the bulges. Again a calculated density map coincided with the lipid distribution. Observed asymmetries could be reproduced if one presumed that lower parts of the 3D structure were embedded in stain material. The missing lipid in the center of the bulges, of course, could also indicate a double helix instead of a quadruple helix. The calculated contour line diagram of such a double helix, however, shows a knot diameter which is too small by 30% and a considerably changed mass distribution pattern.

The pattern originating from the cryomicroscopic CEVS preparation (Figure 3c) also deviates, on first sight, from the quadruple helix structure. One has, however, to take into acount that such electron micrographs represent several different orientations in an ice matrix, which produce an average pattern upon image processing. The latter can be reproduced satisfactorily by averaging over two orientations, namely, the projections at 0° [100] and 45° [110]. Hazy contours as observed experimentally are then obtained (no figure).

We finally turn to the "tubular rod fiber" reproduced in Figure 5. The uniform width of the rod and its striations, all aligned at an angle of 82°, suggest that the rod is built up by a single, tightly coiled helical strand. The pitch (7.4 nm) then corresponds to the regular repeat distance and to the thickness of the fiber. The value of 7.4 nm suggests a 4-fold molecular layer since it corresponds to the length of four molecules. If one presumes that the outer surface of the fiber is hydrophilic, the molecular layers can be arranged in three ways: (i) in two tail-to-tail bilayers (not illustrated), (ii) in one central tail-to-tail bilayer which is surrounded by a monolayer with head-to-tail arrangement (Figure 10, main model), and (iii) in a tetragonal bundle of four tail-to-tail bilayers (Figure 10, lower right). Model i is discarded, because it involves an impossibly tight packing of carbohydrate groups in the fiber's center. Model iii is unlikely, because it should show stained seams

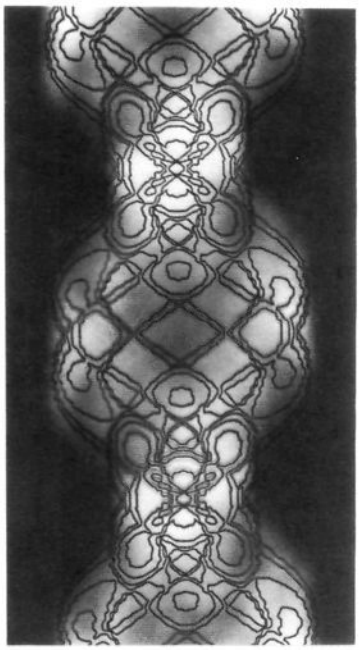

Figure 9. Same diagram as in Figure 8, but for the *N*-dodecylgluconamide (**1b**) fiber depicted in Figure 4b. This fiber is rotated by 45° if compared to the fiber reproduced in Figure 7.

between the individual strands in electron micrographs. They have never been observed although such bundles may occur as short-lived intermediates. We favor model ii because it avoids packing problems, perfectly reproduces the electron micrographs, and contains the head-to-tail arrangement of the final crystals of **1**.

The observed gradient of 82 ± 3° can again be calculated from the same equation which has been used for the quadruple helix: $\tan \Theta = 2\pi \times$ helix radius/pitch $= (2\pi \times 10.0)/7.4 = \tan [8.49]$ or 83.3°. The helix diameter was taken as the difference between the tubule diameter (27.4 nm) minus the strand's thickness (7.4 nm). The same value for the helix radius is also given by the sum of the radii of the central cavity (≈6 nm) and the strand ($6 + 3.7 \approx 9.7$ nm). Simple relationships of the structure parameter are again found:

mol length	strand radius	tube radius	pitch
18.5	37	10.0	7.4
0.5	1	$2 \times \sqrt{2}$	2

If we compare the structure parametrizations given for the quadruple and the tubular helices, we find gradient and pitch ratios of $2\pi : 1$. In addition, strand and the helix radii are both twice as large in the tubular helix as in the strands of the quadruple helix.

Discussion

The probable mechanism of the formation of helical fibers by aggregation of disk micelles has been discussed earlier[3-5] and need not be repeated here. The rearrangement process of the quadruple helix to the tubular helix could not be studied in more detail, because neither the tubular helix nor often observed rope-like intermediate stages could be obtained in pure form. Various supramolecular impurities were always present and prevented solid-state NMR and FTIR studies of these materials in order to compare them with the known spectra of the quadruple helices and crystals.[5] In this section we shall only evaluate the striking geometries of the quadruple 54.7° and single 82° helices. We shall also try to connect both structures.

A four-helix bundle is a common motif in natural proteins and has been recreated in synthetic proteins.[12] These helices are packed nearly (anti) parallel to one another at an angle of 20°. They are stiff and diverge from a point of closest approach giving

(12) Ho, S. P.; De Grado, W. F. *J. Am. Chem. Soc* **1987**, *109*, 6751.

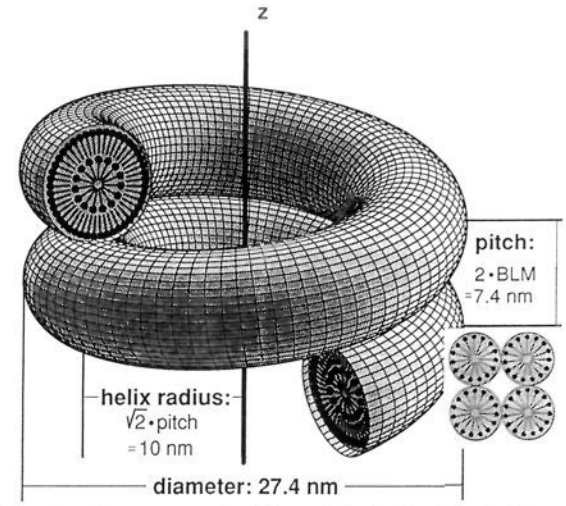

Figure 10. Computer graph of the tubular helix shown in Figure 5 combined with schemes of two possible arrangements of the gluconamide molecules.

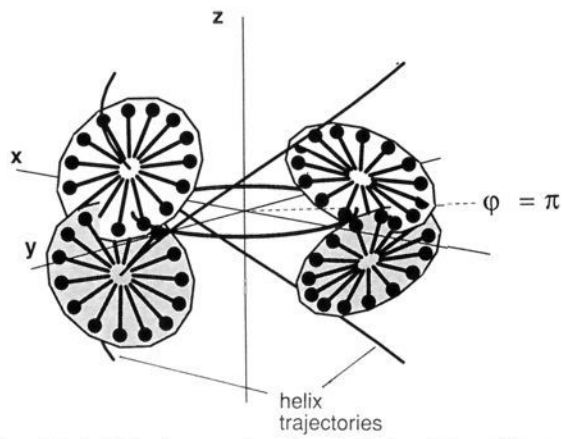

Figure 11. Individual cross sections through the four helices of the model structure given in Figure 7a close to pitch height π. Here the maximal interpenetration of micellar bilayers occurs.

rise to cavities similar to our "bulges". Those portions of the proteins that are in close contact are composed of apolar residues, which often interdigitate. This type of assembly is obviously also formed by the gluconamide micellar fibers, although an open-chain glucose derivative is certainly more polar than a hydrophobic amino acid residue. Nevertheless, crystal structures of *N*-alkylgluconamides show an apolar methylene group at the surface, because the 6-hydroxy group is bent-in to take part in a homodromic hydrogen bond cycle.[7] A detailed analysis of the knot's diameter and shape at $\varphi = 0$ (Figure 7a) indicates that the fibers have to be interdigitated. A sketch of a cross-sectional view (Figure 11) characterizes the situation. Both the polar and unpolar regions must become highly disturbed in the contact region of two helices. This allows the rearrangement of micellar tail-to-tail bilayers to the head-to-tail layers as assumed in the tubular helix (Figure 10) and found in crystals of *N*-octyl-D-gluconamide.[7] The hypothesis of partial head-to-tail arrangements can, in principle, be checked by solid-state NMR spectroscopy since the ^{13}C signal of the terminal CH_3 groups is considerably shifted, if the environment changes from apolar to polar.[5] Both pure (centrifuged) quadruple helices and the crystals thus show only one $^{13}CH_3$ signal, each at $\delta = 15.9$ or 14.4 ppm. It has, however, not been possible to prepare the tubular helices in high concentration in pure form. Crystallization always accompanies the formation of these fibers.

The magic angle can be related to "electric order" phenomena. Durand has recently discussed liquid crystals as oriented quadrupole systems whose gradient creates an order electric polarization $\vec{P}$[13,14] ($\vec{P} = -\vec{\nabla}\ddot{Q}(z)$, where $\vec{\nabla}$ is the Nabla operator and $\ddot{Q}(z)$ is

the quadrupolar density across the layers). The associated quasi-macroscopic dielectric energy is minimal, when the order orientation is oblique at the magic angle ($3\cos^2\Theta - 1 = 0$) compared to the order gradient orientation. This order electricity (i.e., the electric polarization connected with the order gradient) was used to explain observed liquid crystal orientations at SiO needles and other surfaces. In our case, order polarization should arise from the neighboring micellar fibers. Oblique orientation of the single fibers at the magic angle then minimizes the dielectric energy.

The molecular modelling of the helix starting from the monomer is thus not crucial to an understanding of the supramolecular structure. Its incline is obviously caused by a physical phenomenon. This is a fortunate situation, because we found in preliminary calculations on the gluconamide head group that there are at least 10 different conformations possible within an energy range of ±5 kcal/mol. Molecular modelling of the assembly would therefore not have a solid basis.

After discussing the magic angle gradient of the helices, we now turn to the unexpected geometrical relation between strand diameters and pitches. This finding can be rationalized by an application of the Bonnet transformation.[15] This mathematical procedure accomplishes the isometric (i.e., a length and angle preserving) transformation between minimal surfaces. The latter are characterized by a mean curvature of zero, or, in other words, the sum of the two curvatures of two orthogonal surface lines belonging to the same point is zero.

Minimal surfaces were first observed with soap films[15] and were recently found to describe enzyme–substrate interactions in tubular proteins (=van der Waals lens)[16] as well as a glycero monooleate–water cubic structure.[17] Application to the micellar fibers depicted in Figures 7 and 10 involves catenoids and helicoids. Their Bonnet transformation is depicted in Figure 12a. These minimal surfaces are fitted either into the quadruple helices (Figure 12b) or into the helical fiber rods (Figure 12c) simply by scaling the unit surfaces ($r_i = 1$) with the BLM thickness of 3.6 nm. The waist radius of the catenoid is then equivalent to the strand radius of the tubular helix (3.6 nm). The circumference of the waist circle corresponds to the pitch of quadruple helix (22.4 nm). Figure 12b shows the alignment of two helices onto the helicoid surface with a helical radius of $3.6 \times \sinh(1) \times i = 4.23$ nm. i scales the radial extensions of the surfaces and is arbitrarily set equal to 1. Bonnet transformation of the structure given in Figure 7a allows a straightforward construction of the helical tube and the quadruple helix of Figure 10 using the gradient ratio $1{:}2\pi$ (see above).

Furthermore, the gradient Θ is equal to the ratio of torsion τ ($\tau = r/(r^2 + b^2)$) and curvature κ ($\kappa = b/(r^2 + b^2)$; b = pitch$/2\pi$; r = helix radius). The 2π gradient transformation procedure thus provides an elegant approach to discover structural relationships and transitions between molecular assemblies. Attempts to apply the more general topology of zero-potential surfaces[21] are in progress. The reduction of curvature with temperature and time is balanced by an increase in torsion. In the more complex structures displayed in Figure 6c, this trend is continued.

Conclusion

Stereochemical details in glyconamide head groups clearly determine the shape of their supramolecular assemblies. The bend of the gluconamide is, for example, responsible for the formation of helical ropes rather than twisted bilayer sheets or ribbons, which are found for other diastereomers. The homodromic hydrogen bond cycle probably causes a partly hydrophobic surface of the fibers and their assembly to quadruple strands. The fine structure of the helices, however, is clearly dominated by geometrical rules rather than by molecular conformations. These rules are presumably a result of weak repulsion forces between four fibers.

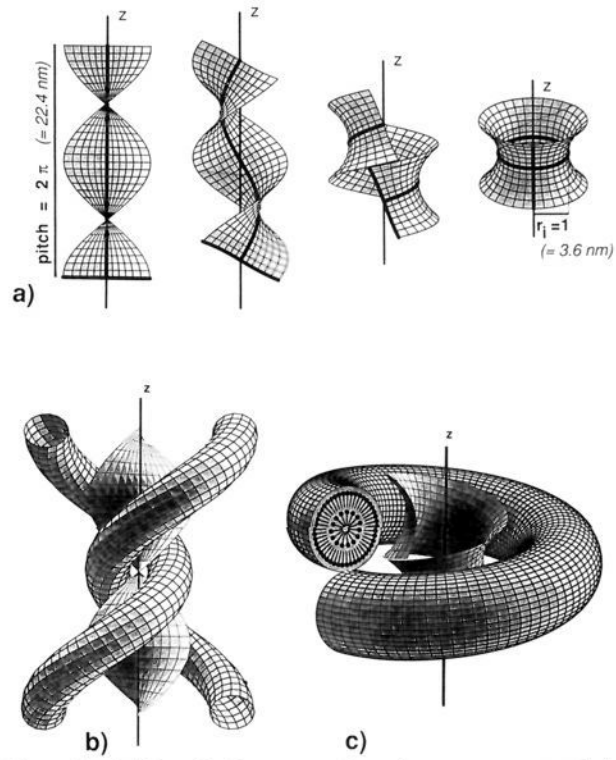

Figure 12. (a) Stepwise Bonnet transformations convert a stretched helicoid to a catenoid. (b) Two opposite strands of the quadruple helix (see Figure 7a) and (c) the tubular helix (see Figure 10) as fitted on Bonnet-related minimal surfaces.

Experimental Section

Gluconamide syntheses are described in detail elsewhere.[3,4] Spectral data (IR, ^{1}H NMR, and MS) and elemental analysis (C, H, N) were in good agreement with the calculated data.

Sample Preparation for Electron Microscopy. (a) Negative Staining. A solution of 1% (w/v) phosphotungstic acid (pH = 7) was mixed with gluconamide (final concentration 0.5% w/v), and the mixture was heated to 100 °C. Upon cooling the hot solution to room temperature, a solid gel formed. Carbon-coated copper grids were dipped into freshly formed gels and excess material was blotted off. The grids were evaluated with Philips EM 400 or Philips CM 12 electron microscopes. The pattern of the micellar fibers on the grid surface was homogeneous and highly reproducible. If 1% (w/v) SDS was added, a quasi-crystalline 2D array of fibers was obtained (Figure 1a). The appearance of other structures as shown in Figure 6 is rare. Aggregation in the presence of phosphotungstic acid always leads to quadruple "bulgy helices". No helical tubes (Figure 5) were observed. If uranyl acetate (1% m/v) instead of phosphotungstic acid was used, the "helical tubes" beside "bulgy helices" became detectable. Presumably a phosphotungstate glass covers freshly formed bulgy helices and protects them from further rearrangements.

(b) Cryomicroscopy. Freeze Etching. A hot 1% (w/v) aqueous solution of the *N*-alkylgluconamides was placed on a copper stub and left to cool to room temperature within 30 min. The stub was mounted on the tweezer of a plunging device and vitrified in liquid ethane (89.7 K). The vitrified sample was freeze etched (Balzers BA 360 M, held at 173 K). Several cuts were made (up to 20) with a cooled microtome (77 K), and the selected smooth surface was etched by leaving the microtome close above the sample. The optimum etching time was 30 s. The sample was immediately shadowed with platinum/carbon (angle = 35°) and carbon (angle = 90°). The replica was cleaned with 50% sulfuric acid and several transfers in double-distilled water. The replica was placed on a copper grid and observed in a Philips EM 300 at 80 kV.

We repeated the above-described procedure several times and obtained the helical tubes in homogeneous distribution and highly reproducible as represented in Figure 5. Occasionally the occurrence of super-coiled helices was observed. Variations of the gluconamide concentration in the

(13) Durand, G. Les Houches Sessions XLVIII; *Liquids and Interfaces*; Elsevier: Amsterdam, 1988; p 633 ff.
(14) Monkade, M.; Boix, M.; Durand, G. *Europhys. Lett.* **1988**, *5*, 697.
(15) (a) Schwarz, H. A. *Mathematische Abhandlungen*; Springer: Berlin, 1890; p 151 ff. (b) Hildebrandt, S.; Tromba, A. *Mathematics and Optimal Form*; W. H. Freeman, Scientific American Library: New York, 1985. (c) Andersson, S.; Hyde, S. T.; Larsson, K.; Lidin, S. *Chem. Rev.* **1988**, *88*, 221–242.
(16) Hyde, S. T.; Andersson, S. *Z. Kristallogr.* **1986**, *174*, 225.
(17) Blum, B.; Lidin, S.; Andersson, S. *Angew. Chem.* **1988**, *100*, 995.

applied range of 0.5–2% did not influence the appearance of the structures.

CEVS Preparation. The controlled environment vitrification system (CEVS), described by Bellare et al.[9] and routinely being used at the Technion in Haifa, allows the sample preparation in an isolated chamber under controlled temperature and solvent saturation. The conditions defined for our experiments were water vapor saturation at 70 °C. This temperature is slightly below the melting point of the gel. A droplet of the sample was placed onto the "holey" carbon-coated grid held by a tweezer of the plunging device. The excess fluid was blotted off and the grid was rapidly plunged through a shutter opening into a cryogenic bath of ethane (89 K). The vitrified sample was observed in the electron microscope (JEOL 100 CX, 100 kV) using a Gatan cold stage (Gatan 623-3).

The concentration of *N*-octylgluconamide was 0.5% (w/v) in water. Statistically arranged helical fibers were found, if the CEVS apparatus was kept at 70 °C. At 50 °C partial rearrangement to the helical tubes characterized by freeze-etching procedures (Figure 5) occurred. Higher concentrations did not yield thin enough films; lower concentrations (e.g., 0.3% w/v) gave the same results. Adding 1% w/v SDS to the 0.4% solution yielded parallel ordering of the fibers (Figure 3).

Image Analysis. The micrographs were digitalized with a CCD camera (Datacopy 610F, Long Beach, CA). The scanning step size was 25.6 μm, which corresponds to a pixel size of 557 pm at a magnification of 46 000. Identical motifs were averaged by a correlation method, which is not strictly dependent on regular periods.[18] A reference motif was cross-correlated with the digitized image. Points of good correlation, corresponds to local maxima of the cross-correlation function, indicated the location of the motifs. Small sections of the image were now averaged by superposition. This average image served as new reference in a further iteration step.

The 3D reconstruction was obtained from 14 tilted (−56° to 48°; 8° steps) and averaged images. The latter was calculatd from 165 single motifs each. The method has been applied for 2D crystals.[19] It was adjusted to the fact that the relative positions of fibers varied and only one periodicity along the fiber axis occurred. The results of the analysis verified the impression already obtained from visual inspection of the micrographs, namely, a substantial flattening of the preparation. This is particularly prominent at high tilt angles; the fibers become narrower. A comparison with the model data is most meaningful in the 0° projection.

The specification of measurements and related errors are given as follows. The main error in measurement occurs from deviation of the magnification, which may lie in the order of up to 10% (manufacturers specification). Therefore, it is useful to determine the actual value of the magnification. We used carbon black (lattice parameter 0.34 nm) as the standard and obtained the value of magnification from laser-optical diffractograms. The corrected values were used for the determination of the measured parameters.

Furthermore, we wish to mention that the extractable resolution in negative-stained samples is usually limited to 2 nm. Therefore, we are not able to give any direct information at the molecular level from the micrographs or image processed pattern. The final image pattern shown in Figure 1, b and c, is an average of 165 individual motifs, extracted from the EM image by applying the cross-correlation technique. The permitted deviation from the reference motif was 2%. Data of the tubular helix were directly taken from electron micrographs, such as given in Figure 5.

Modelling. Judgement by eye and use of geometrical instruments allowed the determination of the central axes in the contour line diagrams of both quadruple helices (Figures 1c and 4b). The more difficult assignment of the radial limits was accomplished as follows. A level curve at the foot of the steepest ascent and at approximately one-third of the distance between the minima and maxima of the mass distribution was selected. It was marked with a white line parallel to the central axis (see Figures 1c and 4b). This procedure was substantiated and refined by the application of two geometric approximations. We first treated the fiber as a tilted cylinder with a circular or elliptical cross section. The mass distribution within this cross section is then reproduced by the area under an inversed parabola of the form $y = 2b[(1 - x^2)/a^2]^{1/2}$ (y = height; a, b = elliptical radii). The intersections with the x-axis (=surface of the grid) thus define the outer limits of the lipid fiber. In a second step, we compared this purely geometrical function with the Gauss distribution function $y = \sqrt{(\alpha/\pi)}\exp(-\alpha r^2)$ (r = radial distribution), which should be more realistic for a lipid fiber deformed by gravity and adsorption forces. For this purpose we scaled the parabola to make the integral over the fiber diameter (=2a) equal to 1. The Gauss distribution curve was fitted to the profile line pattern by its slope parameter α. Superposition of both functions shows that the desired radius cuts the Gauss function always in the region between 25 and 35% of the total height. The determined radial data varied by ±5%.

Fiber arrangements and their orientations with respect to the z-axis were found by extensive use of computer-aided visual representation. For this purpose, a program allowing interactive study of all relevant parameters, such as the pitch, the radii, and particularly the lateral and angular arrangements of individual helical strands was developed in FORTRAN 77 (IBM RT50/AIX; GDT: graphics development tool kit). A set of 3D graphic transformation routines as well as routines for the representation of different picturing modes, partially animated, and structure sections provided necessary and helpful tools.

Detailed structural analyses were worked out using MATHEMATICA® (Wolfram Research; Macintosh II si and SUN Spark station 4). These included, among others, cross-sectional and density profile calculations of the model structures and a number of related structures with different parameter sets and fiber arrangements. The inclination angle Θ, for example, was varied. Significant deviations between the model contour line diagram and the electron micrographs became, for example, obvious at 52° and 57°. More details will be described in a technical paper.

The calculations of the presented fiber structures were performed using the numerical model relationships given below. Since the pitch was the most reliable value obtained in each case, all the data were derived from it. For the octyl [dodecyl] gluconamide quadruple helices, the following data were used: pitch 22.4 [27.1] nm, molecular length 1.78 [2.15] nm, bulge radius 2.50 [3.05] nm, helix radius 5.04 [6.10] nm.

Using the numerical relationships between the gradients and the pitches (2π : 1) given for the supposed structure transition from the quadruple helices to the tubular helix, the following data emerge (in parentheses, measured values): pitch = 2 × BLM = 7.13 (7.4) nm, helix radius = 10.08 (10.0) nm, gradient = $2\pi \times \sqrt{2}$ = 8.885 or 83.6° (7.11 or 82°).

The calculations of the cross-sectional densities were carried out on the basis of the undistributed 3D structure as depicted in Figure 7a,b and the adequately scaled structure of the C-12 homologue which is turned by 45° around the z-axis. Since all of the circular, molecular layers are tilted corresponding to the helical gradient, the layer densites were calculated from the intersection lengths of elliptical planes (long axis a = BLM/cos (gradient), short axis b = BLM) with an integer grid (point distances 0.20 nm) perpendicular to the z-axis. The profile then resulted from scanning the layer densities of the ellipses which are rotationally aligned around the individual helical z-axes. The densities were compared to the lipid distribution of the Fourier-analyzed electron micrographs (Figure 1b) by an overlay of their contour line representation (Figure 8).

Acknowledgment. This work was supported by the Sonderforschungsbereich 312 "Vectorial Membrane Processes" of the Deutsche Forschungsgemeinschaft, the Förderungskommission of the Freie Universität Berlin, and the Fonds der Chemischen Industrie. Professor Dr. S. Grund and J. Gatzmann provided the freeze-etching apparatus as well as excellent technical support. K. Weiss helped with the tilting experiments.

(18) Saxton, W. O.; Baumeister, W. *J. Micros. (Oxford)* **1982**, *127*, 127.
(19) Saxton, W. W.; Baumeister, W.; Hahn, M. *Ultramicroscopy* **1984**, *13*, 57.
(20) Nitsche, J. C. C. *Vorlesungen über Minimalflächen*; Springer: Berlin, 1975.
(21) von Schnering, H. G.; Nesper, R. *Angew. Chem., Int. Ed. Engl.* **1987**, *26*, 1059–1080.